Front. Mater. Sci. 2014, 8(3): 256–263
DOI 10.1007/s11706-014-0259-3

RESEARCH ARTICLE

Effect of different processings on mechanical property and corrosion behavior in simulated body fluid of Mg–Zn–Y–Nd alloy for cardiovascular stent application

Shi-Jie ZHU (✉)[1], Qian LIU[1], Ya-Feng QIAN[2], Bin SUN[1], Li-Guo WANG[1], Jing-Min WU[2], and Shao-Kang GUAN (✉)[1]

1 School of Materials Science and Engineering, Zhengzhou University, 100 Kexue Road, Zhengzhou 450001, China
2 National Centre for Quality Supervision and Inspection of Magnesium and Magnesium Alloy Product, No. 1 Xing He Street, Hebi 458000, China

ABSTRACT: The biomagnesium alloys have been considered to be one of the most potential biodegradable metal materials due to its good mechanical compatibility, biological compatibility, biological security and biodegradable characteristics. However, the two major problems of high degradation rates in physiological environment and low mechanical properties prevent the development of biomagnesium alloys. In the present work, the samples of Mg–Zn–Y–Nd alloy were prepared by cyclic extrusion compression (CEC) and equal channel angular pressing (ECAP). The microstructures, mechanical properties of alloy and its corrosion behavior in simulated body fluid (SBF) were evaluated. The results reveal that Mg–Zn–Y–Nd alloy consists of equiaxial fine grain structure with the homogeneous distribution of micrometer size and nano-sized second phase, which was caused by the dynamic recrystallization during the ECAP and CEC. The corrosion resistance of alloy was improved. The tensile and corrosion resistance were improved, especially the processed alloy exhibit uniform corrosion performances and decreased corrosion rate. This will provide theoretical ground for Mg–Zn–Y–Nd alloy as vascular stent application.

KEYWORDS: cyclic extrusion compression; equal channel angular pressing; extrusion; magnesium alloy; corrosion

Contents

Received June 27, 2014; accepted July 29, 2014

E-mails: skguan@zzu.edu.cn (S.K.G), zhusj@zzu.edu.cn (S.J.Z)

1 Introduction

In recent years, magnesium and its alloys have been suggested an innovative biodegradable metallic implant materials for biomedical applications owing to the lower density, higher specific strength and an elastic modulus closer to that of human bone [1]. In addition, it is desirable to use materials that can degrade in the physiological environment so that a subsequent surgical procedure is not necessary to remove the implants from the human body after the tissues have healed [2]. However, the practical use of biomedical magnesium alloys faces some challenges, such as inherent low strength and fast corrosion rate. It has been reported that Mg–Zn alloy losses over 30% bending strength with about 6% weight loss [3] and pure Mg losses 70% compressive yield strength with approximately 3% weight loss [4]. In addition, the fast corrosion of magnesium alloys, leading to mismatch of tissue healing rate and the gas cavity around the implants [3,5], also need to be tailored. Therefore, it is necessary to improve the mechanical properties and corrosion resistance.

The beneficial effect of grain refinement on mechanical properties and corrosion resistance of Mg alloys have been widely investigated [6–11], especially when exploiting severe plastic deformation (SPD) techniques to produce ultrafine-grained (UFG) materials featuring a submicrometer grain size [6–10]. Typical SPD techniques currently in use include equal channel angular pressing (ECAP), high pressure torsion (HPT) and cyclic extrusion compression (CEC) etc. [12]. UFG Mg alloys by SPD can result in a more uniform distribution of intermetallic particles, which is an important factor responsible for the improved corrosion resistance [11]. Gao et al. [13] reported that UFG bulk Mg–Zn–Ca alloy processed by HPT exhibited uniform corrosion owing to the homogeneous distribution of nano-sized second phase, but unsuitable for vascular stent application because of their small size. Gu et al. [14] indicated that as-ECAPed AZ31 alloy presented similar corrosion rate with sized corrosion pits on the surface much smaller than that of the as-extruded one. Wu et al. [15] has reported the CEC treated samples showed homogeneous corrosion because of the grain refinement and the homogeneous distribution of nano-sized second phase. However, limited studies focused on the corrosion behavior of Mg alloy processed by different SPD methods. However, Song et al. [11,16] indicated that the dependence of corrosion rate on grain size is actually non-monotonic. Magnesium grains show anisotropic corrosion behavior and different corrosion performance depending on its crystallographic orientation of the grains in the single-phase, hot-rolled AZ31 sheet with a great deal of texture.

The aim of this study is to investigate the mechanical property and corrosion behavior of the Mg–Zn–Y–Nd alloy processed by CEC, ECAP and hot extrusion. Accordingly, the present research is initiated to determine whether the grain size is the predominant factor in controlling the corrosion response, and to what extent the corrosion resistance of Mg–Zn–Y–Nd alloy can be altered by SPD processing.

2 Experimental

2.1 Materials

A Mg–Zn–Y–Nd alloy ingot was prepared with high purity Mg, high purity Zn, Mg–25Y (wt.%, 99.99% in purity) and Mg–25Nd (wt.%, 99.99% in purity) master alloys through induction in a mild steel crucible at approximately 740°C under CO_2/SF_6 (Vol. 3000:1) atmosphere in an electronic resistance furnace. Then, the as-cast ingot was directly extruded at 320°C with an extrusion ratio of 36:1 and a ram speed of 1 mm/s.

In the CEC processing, the samples (30 mm × 42 mm) machined from the ingot were extruded by 4 passes. The die was illustrated in Ref. [17]. The CEC processing was carried out by pushing a specimen from one cylindrical chamber with a diameter D, into the second chamber with the same dimensions, through a die having a smaller diameter d. In the present study, D and d were 30 and 20 mm, respectively. The temperature was 320°C and the ram speed was 5 mm/s. During the final extrusion pass, the opposite ram was removed in order to release the rod.

This rod was machined into cuboids for ECAP experiment with a dimension of 12 mm × 12 mm × 90 mm. The die consists of two cross channels, intersecting at an angle of 90° between the vertical and cross channels. The extrusion route was Bc [18], rotating 90° clockwise along its longitudinal axis between adjacent passes. In order to prevent crack deformation, the ECAP experiment should be performed at high temperature, the die was preheated to 380°C, and the samples was brushed with a layer of graphite and heated to 370°C in holding furnace. After reaching the temperature, the sample was pressed for 4 passes with an extrusion speed of 3 mm/s.

2.2 Microstructural observation

Microstructural characterization of specimens was observed through optical microscopy (OM; Olympus, H2-UMA) and scanning electron microscopy (SEM; Philips, Quanta-2000). Specimens for OM and SEM were prepared by mechanical polishing and etching using a solution consisting of 4.2 g picric acid, 10 mL acetic acid, 70 mL ethanol, and 10 mL water. Average grain size was measured according to the linear intercept method described in the ASTM standard E112-G6.

2.3 Mechanical properties test

The tensile tests (specimens with a gauge length of 8 mm and cross-sectional areas of 3 mm × 1.5 mm) were conducted on a SHIMADZU AG-IC 50KN test machine at room temperature with a strain rate of 1 mm/min. The fracture morphology was observed by SEM mentioned above.

2.4 Corrosion tests

Electrochemical measurements were carried out with a traditional three-electrode cell on an electrochemical workstation (Metrohm-Autolab, PGSTAT 302N). A disk-shaped sample with a diameter of 10 mm and a thickness of 2 mm, a platinum electrode and a saturated calomel electrode were set as the working electrode, the auxiliary electrode and the reference electrode, respectively. All the measurements were made at a temperature of (37±0.5)°C in simulated body fluid (SBF) solution [19] with a pH value of 7.4. An average of at least three measurements was taken for each group.

Immersion tests were carried out in SBF according to the ASTM-G31-72 standard. Disk-shaped samples with a diameter of 10 mm and a thickness of 3 mm were immersed in 50 mL SBF solutions and the temperature was maintained at 37°C with a water bath. After 30-day immersions, samples were taken out of SBF, gently rinsed with distilled water and dried in the vacuum oven. After the immersion test, the corrosion products were removed in chromic acid solution (200 g/L Cr_2O_3 + 10 g/L $AgNO_3$). The volume of hydrogen generated from the reaction between the Mg–Zn–Y–Nd alloy and SBF was monitored in accordance with Ref. [20].

3 Results and discussion

3.1 Microstructural characterization

Figure 1 shows the optical microstructures of as-CECed, as-ECAPed and as-extruded Mg–Zn–Y–Nd alloy. The microstructures of the as-CECed and as-ECAPed alloy are dynamic recrystallized and contain equiaxed grains of α-Mg and fine micrometer sized particles, as shown in longitudinal directions in Figs. 1(a) and 1(b). It is reported that the second phase was $Mg_{12}Nd$ phase identified by the X-ray diffraction (XRD) measurement [15]. After 4 passes of CEC treatment, the microstructure of the alloy became finer and more homogenous due to the dynamic recrystallization occurred during the deformation. The grain size was refined to about 1 μm and the second phase $Mg_{12}Nd$ distributed in the grains and along the grain boundaries which were brittle and formed into a cluster, as shown in Fig. 2(a). Obviously, we can find that the average grain size of the as-ECAPed alloy was ~20 μm owing to the much higher processing temperature. At the same time some the second phase which came from the cluster phase uniformly precipitated in grains, as shown in Fig. 2(b). Because it is much easier to appear cracks in the ECAP treatment at the low temperatures, we had to improve the test temperature to obtain the available samples. Therefore, the grain had

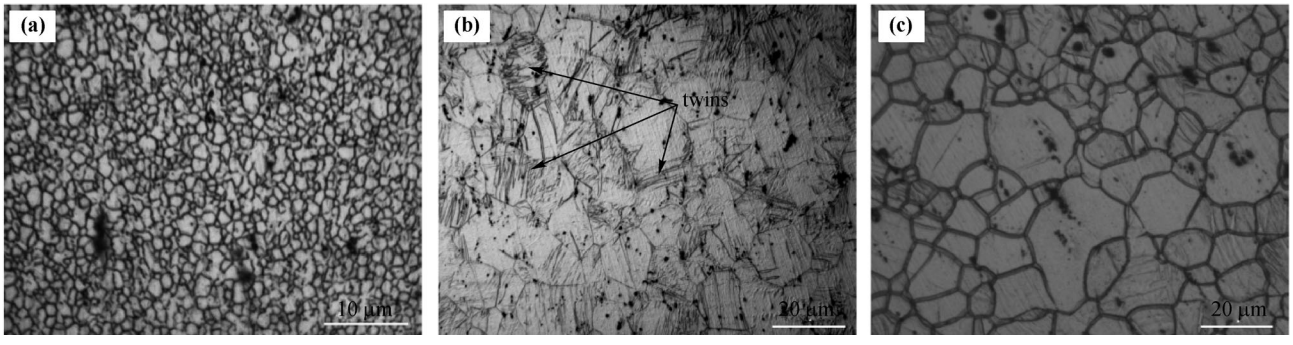

Fig. 1 Longitudinal microstructures of Mg–Zn–Y–Nd alloy: **(a)** as-CECed; **(b)** as-ECAPed; **(c)** as-extruded.

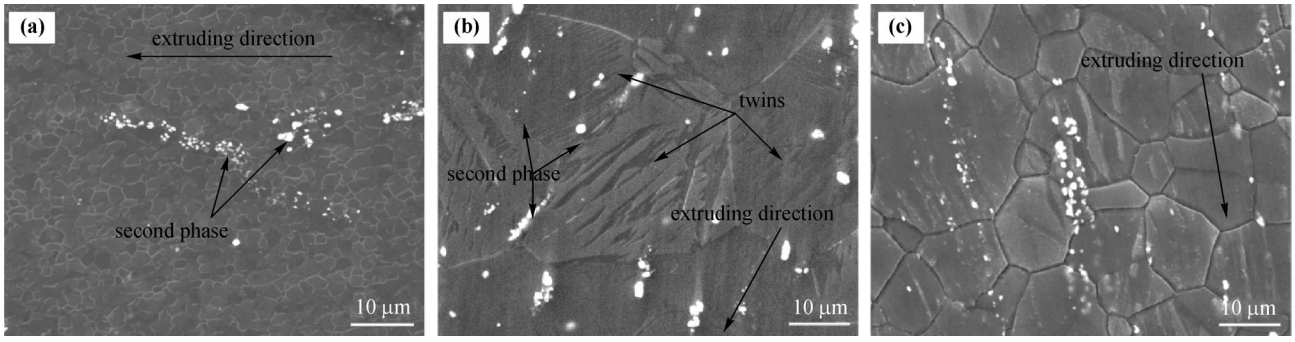

Fig. 2 Distribution of second phase: **(a)** as-CECed; **(b)** as-ECAPed; **(c)** as-extruded.

been grown greatly at elevated temperature. In addition, a small amount of the deformation twins were found in Figs. 1(b) and 2(b). It has been reported that the $\{10\bar{1}2\}$ extension twins have been found to occur most frequently during large deformation of magnesium alloys [21]. The microstructure of the as-extruded alloy was heterogeneous, which was the typical microstructure of incompletely dynamic recrystallized alloys, as shown in Fig. 1(c). Coarse grains of ~15 μm in size were surrounded by fine dynamic recrystallized grains of 5–8 μm in size. The long elongated grains in as-extruded alloy (Fig. 1(c)) were suggested to appear from previous unextruded microstructures that have survived from dynamic recrystallization [22]. The second phase distributed gathered in the grains and even along the grain boundaries, as shown in Fig. 2(c).

A refined and homogenous microstructure of as-CECed samples was obtained, ascribed to the dynamic recrystallized microstructure that would not obviously grow due to plastic deformation occurred below the dynamic recrystallization temperature. Moreover, the grains and the second phase were brittle under the pressure of extrusion and compression during the CEC processing. Although the grain size of as-ECAPed alloy was larger than that of as-extruded, it can exhibit more uniform and refined microstructures in both directions, especially in the longitudinal section.

3.2 Mechanical properties

Figure 3 shows the mechanical properties of Mg–Zn–Y–Nd alloy with different processes. The obtained average yield strength (YS), ultimate tensile strength (UTS) and elongation (EL) to failure are summarized in Table 1. It is apparent that the EL values of as-CECed and as-ECAPed samples are much higher than those of as-extruded (with an improvement of ~41% and ~44%, respectively). The result indicates that the SPD processing plays a significant role in

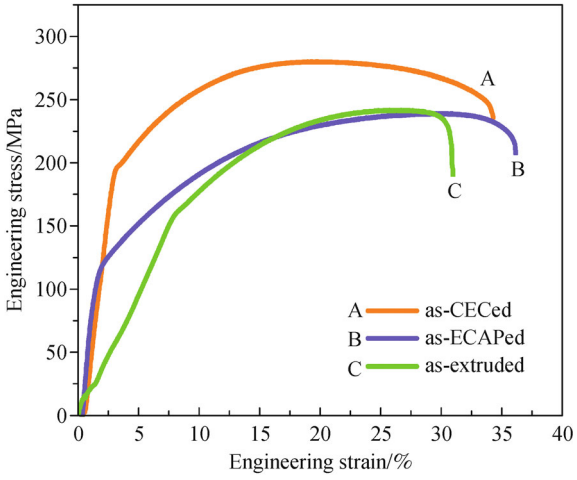

Fig. 3 Stress–strain curves of the Mg–Zn–Y–Nd alloys.

Table 1 Tensile properties of the Mg–Zn–Y–Nd alloy

Sample	YS /MPa	UTS /MPa	δ /%
CEC	194	280	29.4
ECAP	96	239	30.1
Hot extrusion	170	242	20.9

ductility improvement. As for CEC treated alloy, the $Mg_{12}Nd$ phase precipitated, which is beneficial for the enhancement in strength of the alloy [23]. Therefore, the improvement of the strength is mainly due to the grain refinement and precipitation strengthening.

However, UTS clearly presents an inverse relationship after ECAP and hot extrusion treatments. The average grain size of as-ECAPed alloy is larger than that of as-extruded, but the UTS value of as-ECAPed alloy is close to that of hot extruded alloy. It means that the strength of Mg–Zn–Y–Nd alloys is affected not only by grain size but also by dislocation density, texture and grain-boundary microstructure, as has been reported in Ref. [16]. In this case, the deformation twins have been found to occur most

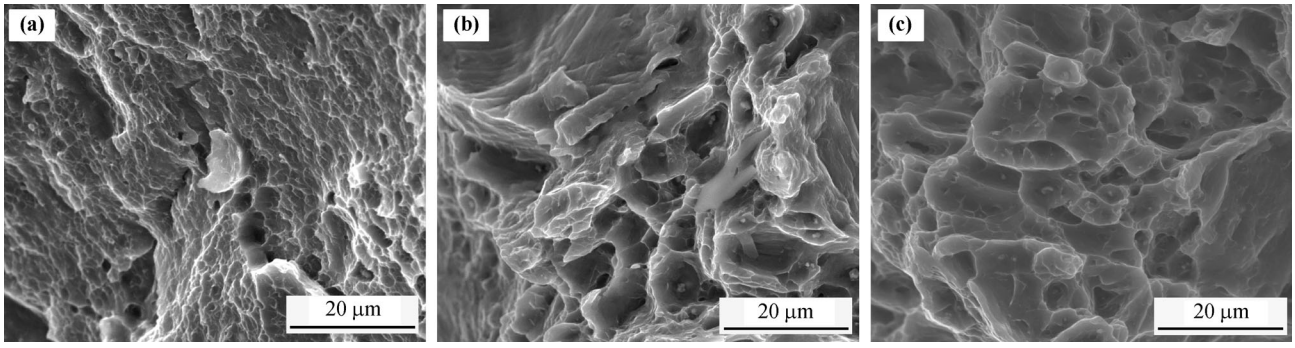

Fig. 4 Fracture surfaces of Mg–Zn–Y–Nd alloys: **(a)** as-CECed; **(b)** as-ECAPed; **(c)** as-extruded.

frequently during large deformation of as-ECAPed alloy, as shown in Figs. 1(b) and 2(b). In principle, homogeneous deformation of a polycrystalline material requires at least 5 independent slip systems. However, magnesium has only 2–3 independent slip systems at room temperature, which is insufficient to satisfy the von Mises criterion. Therefore, coarse-grained hexagonal close-packed (hcp) metals usually need twinning to accommodate plastic deformation in addition to dislocation slip due to their insufficient slip systems.

Figure 4 shows typical SEM images of the fracture surfaces of the Mg–Zn–Y–Nd alloy produced by different processes. All the samples showed dimples — the typical feature of a ductile fracture. However, the as-CECed and as-ECAPed samples exhibited obviously uniform deformation characteristics. For as-CECed sample, it can be concluded that the main contributors to the high elongation are grain refinement and the precipitated second-phase particles of $Mg_{12}Nd$. Therefore the finer and more homogeneous microstructure increased activation of non-basal slip systems and grain boundary sliding [16]. For as-ECAPed sample, since the formation of twin crystals, the crystallographic directions are altered, which results in the transformation of slip system. In addition, the slip system transferred to the advantageous site can promote the further slip and the deformation of crystals. Greater deformation can be obtained by the interaction of twins and slip.

3.3 Corrosion behavior

Figure 5 presents the Tafel curves of electrochemical samples. The electrochemical data of Mg–Zn–Y–Nd alloy in SBF are summarized in Table 2. It can be seen that the corrosion potential (E_{corr}) of as-CECed alloy shifted to a more positive value than that of the as-ECAPed and as-extruded ones, and the corrosion current density (I_{corr}) of the alloy decreased from 0.139 to 0.099 mA/cm^2.

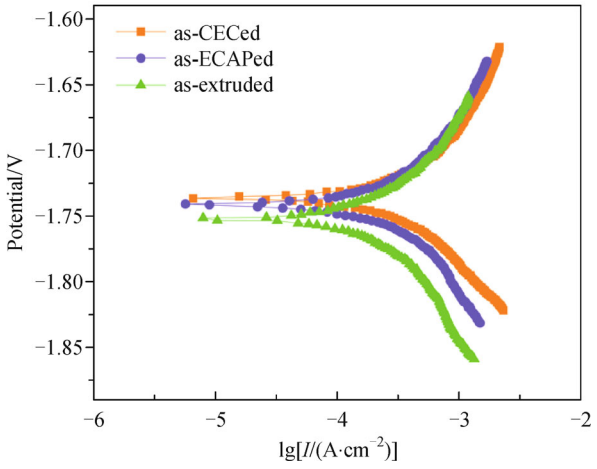

Fig. 5 Polarization curves of Mg–Zn–Y–Nd alloy in SBF.

Table 2 Electrochemical data of Mg–Zn–Y–Nd alloy in SBF

Processing	E_{corr} /V	I_{corr} /(mA·cm^{-2})
CEC	−1.736	0.099
ECAP	−1.742	0.108
Hot extrusion	−1.753	0.139

Note: E_{corr}— corrosion potential; I_{corr}— corrosion current density.

Figure 6 indicates the change of hydrogen evolution rate and corrosion rate of Mg–Zn–Y–Nd alloy during the immersion period. Since magnesium alloys are relatively reactive metallic materials, once implanted *in vivo* or immersed in SBF, they will react with the surrounding medium, generating the following corrosion products: released Mg^{2+} and alloying element metal ions, hydrogen bubbles, solution alkalization caused by OH^- ions and peeled-off particulates. In the present study, the as-CECed alloy exhibited uniform corrosion features during the immersion tests. The corrosion rates of the as-CECed and as-ECAPed alloys show respectively ~27.5% and ~5.7% decreased compared with as-extruded, according to hydrogen evolution experiments. Moreover, the corrosion

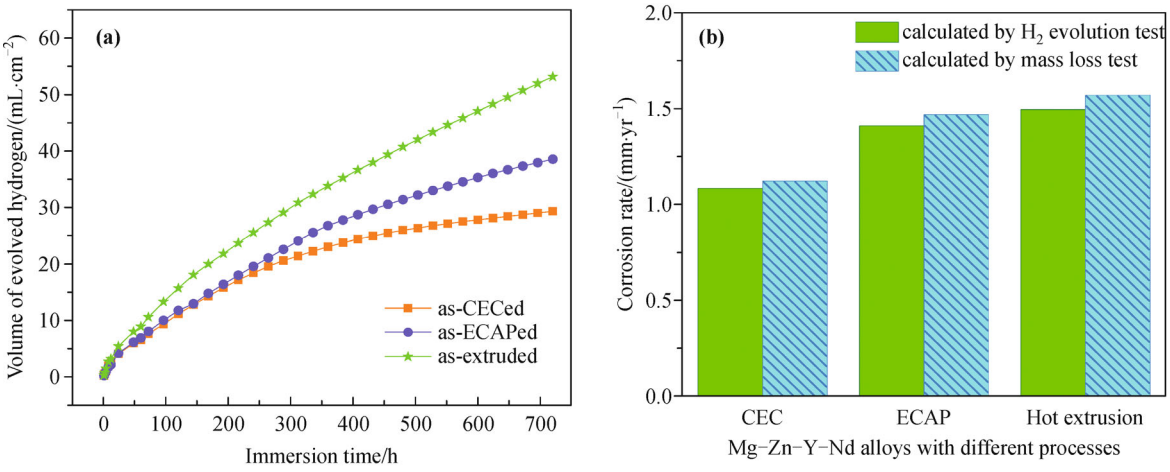

Fig. 6 **(a)** Hydrogen evolution curves. **(b)** A comparison between hydrogen evolution and weight loss of corrosion rate of Mg–Zn–Y–Nd alloys.

rates of all the samples obtained from hydrogen evolution experiment are a little slower than those obtained from mass loss experiment. The reason was probably that some hydrogen released into the air during renewing SBF and some dissolved into the immersion solution, which could not be collected.

The corrosion microtopographies of Mg–Zn–Y–Nd alloy after removing the corrosion products are shown in Fig. 7 and their surface macro-morphologies after immersion in SBF for 720 h show in Fig. 8. There are a lot of tiny pits which distribute uniformly on the surface of the alloy. Furthermore, for the finer microstructure, as-CECed and as-ECAPed alloy presents much tinier and more homogenous pits than as-extruded ones. Corrosion pitting was observed apparently in the as-extruded alloy, while the others show a flat surface, especially in the as-CECed alloy.

The hydrogen evolution test proved that the as-CECed alloy was the most corrosion-resistant material, with a calculated corrosion rate of 1.0837 mm/yr. From Fig. 6, it can be seen that the as-CECed alloy shows the minimum hydrogen evolution rate after 30 d immersion in SBF, which was in agreement with the results of the electrochemical results. One main reason for this result is that the grain size of the alloy was strongly refined during the CEC processing, and the small grain size creates more grain boundaries that act as a corrosion barrier to increase the corrosion resistance [6,11]. It has been reported that grain refinement can improve material's corrosion resistance, resulting in decreased general corrosion rate and alleviation of corrosion localization [7]. It is interesting to find slightly enhanced corrosion of as-ECAPed alloy than that of as-extruded alloy, which is likely attributed to the uniform microstructures.

4 Conclusions

1) The microstructures of as-CECed and as-ECAPed Mg–Zn–Y–Nd alloy were dynamically recrystallized and contained equiaxed grains of α-Mg and micrometer sized

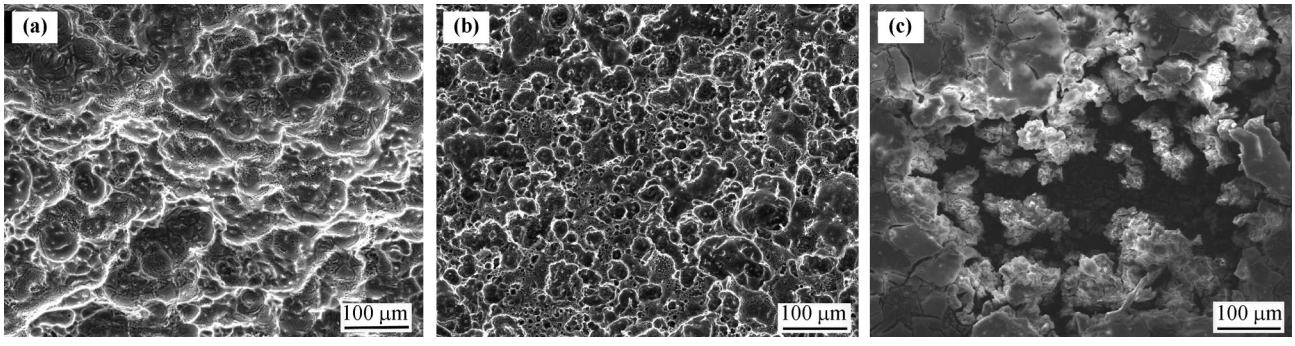

Fig. 7 Surface micro topographies of Mg–Zn–Y–Nd alloy after immersion in SBF solution at 37°C for 720 h: **(a)** as-CECed; **(b)** as-ECAPed; **(c)** as-extruded.

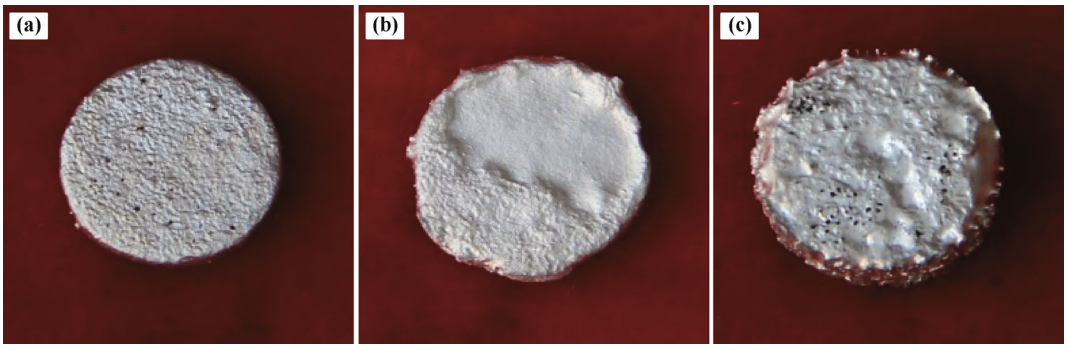

Fig. 8 Surface macro-morphologies of Mg–Zn–Y–Nd alloy after immersion in SBF solution at 37°C for 720 h: **(a)** as-CECed; **(b)** as-ECAPed; **(c)** as-extruded.

particles. A homogeneous microstructure of refined grains with a size of ~1 μm was obtained after 4-passes CEC processing.

2) The mechanical properties of the alloy were greatly improved after the CEC processing. After 4-passes CEC, the EL to failure of the alloy reached up to 29.4%, accompanied by an increase in YS and UTS.

3) The as-CECed and as-ECAPed samples exhibited uniform corrosion due to the homogeneous microstructure; especially the as-CECed Mg–Zn–Y–Nd alloy shows the minimum hydrogen evolution rate of 1.0837 mm/yr.

Abbreviations

CEC	cyclic extrusion compression
ECAP	equal channel angular pressing
EL	elongation
HPT	high pressure torsion
OM	optical microscopy
SBF	simulated body fluid
SEM	scanning electron microscopy
SPD	severe plastic deformation
UFG	ultrafine-grained
UTS	ultimate tensile strength
XRD	X-ray diffraction
YS	yield strength

Acknowledgements The authors are grateful for the support by National Key Technology R&D Program of China (Grant No. 2012BAI18B01) and the National Natural Science Foundation of China (Grant No. 51171174).

References

[1] Wen Z H, Wu C J, Dai C S, et al. Corrosion behaviors of Mg and its alloys with different Al contents in a modified simulated body fluid. Journal of Alloys and Compounds, 2009, 488(1): 392–399

[2] Witte F, Hort N, Vogt C, et al. Degradable biomaterials based on magnesium corrosion. Current Opinion in Solid State and Materials Science, 2008, 12(5–6): 63–72

[3] Zhang S, Zhang X, Zhao C, et al. Research on an Mg–Zn alloy as a degradable biomaterial. Acta Biomaterialia, 2010, 6(2): 626–640

[4] Gu X N, Zhou W R, Zheng Y F, et al. Degradation and cytotoxicity of lotus-type porous pure magnesium as potential tissue engineering scaffold material. Materials Letters, 2010, 64 (17): 1871–1874

[5] Li Z, Gu X, Lou S, et al. The development of binary Mg–Ca alloys for use as biodegradable materials within bone. Biomaterials, 2008, 29(10): 1329–1344

[6] Hamu G B, Eliezer D, Wagner L. The relation between severe plastic deformation microstructure and corrosion behavior of AZ31 magnesium alloy. Journal of Alloys and Compounds, 2009, 468(1–2): 222–229

[7] Yamashita A, Horita Z, Langdon T G. Improving the mechanical properties of magnesium and a magnesium alloy through severe plastic deformation. Materials Science and Engineering A, 2001, 300(1–2): 142–147

[8] Alvarez-Lopez M, Pereda M D, del Valle J A, et al. Corrosion behaviour of AZ31 magnesium alloy with different grain sizes in simulated biological fluids. Acta Biomaterialia, 2010, 6(5): 1763–1771

[9] Xia K, Wang J T, Wu X, et al. Equal channel angular pressing of magnesium alloy AZ31. Materials Science and Engineering A, 2005, 410–411(S1): 324–327

[10] Jin L, Jin D L, Mao D L, et al. Microstructure evolution of AZ31 Mg alloy during equal channel angular extrusion. Materials Science and Engineering A, 2006, 423(1–2): 247–252

[11] Song G L, Xu Z. Effect of microstructure evolution on corrosion of different crystal surfaces of AZ31 Mg alloy in a chloride containing solution. Corrosion Science, 2012, 54: 97–105

[12] Estrin Y, Vinogradov A. Extreme grain refinement by severe plastic deformation: A wealth of challenging science. Acta

Materialia, 2013, 61(3): 782–817

[13] Gao J H, Guan S K, Ren Z W, et al. Homogeneous corrosion of high pressure torsion treated Mg–Zn–Ca alloy in simulated body fluid. Materials Letters, 2011, 65(4): 691–693

[14] Gu X N, Li N, Zheng Y F, et al. *In vitro* study on equal channel angular pressing AZ31 magnesium alloy with and without back pressure. Materials Science and Engineering B, 2011, 176(20): 1802–1806

[15] Wu Q, Zhu S, Wang L, et al. The microstructure and properties of cyclic extrusion compression treated Mg–Zn–Y–Nd alloy for vascular stent application. Journal of the Mechanical Behavior of Biomedical Materials, 2012, 8: 1–7

[16] Song G L. Effect of texture on the corrosion behavior of AZ31 Mg Alloy. JOM, 2012, 64(6): 671–679

[17] Lin J B, Wang Q D, Peng L M, et al. Microstructure and high tensile ductility of ZK60 magnesium alloy processed by cyclic extrusion and compression. Journal of Alloys and Compounds, 2009, 476(1–2): 441–445

[18] Segal V M. Equal channel angular extrusion: from macromechanics to structure formation. Materials Science and Engineering A, 1999, 271(1–2): 322–333

[19] Kokubo T, Takadama H. How useful is SBF in predicting *in vivo* bone bioactivity? Biomaterials, 2006, 27(15): 2907–2915

[20] Song G L, Atrens A. Understanding magnesium corrosion — A framework for improved alloy performance. Advanced Engineering Materials, 2003, 5(12): 837–858

[21] Jiang L, Jonas J J, Luo A A, et al. Influence of $\{10\bar{1}2\}$ extension twinning on the flow behavior of AZ31 Mg alloy. Materials Science and Engineering A, 2007, 445–446: 302–309

[22] Bohlen J, Yi S B, Swiostek J, et al. Microstructure and texture development during hydrostatic extrusion of magnesium alloy AZ31. Scripta Materialia, 2005, 53(2): 259–264

[23] Zhang X B, Yuan G Y, Mao L, et al. Effects of extrusion and heat treatment on the mechanical properties and biocorrosion behaviors of an Mg–Nd–Zn–Zr alloy. Journal of the Mechanical Behavior of Biomedical Materials, 2012, 7(SI): 77–86